Improved Estrogen Receptor Assessment by PET Using the Novel Radiotracer ^{18}F-4FMFES in Estrogen Receptor–Positive Breast Cancer Patients: An Ongoing Phase II Clinical Trial

Michel Paquette, Éric Lavallée, Serge Phoenix, René Ouellet, Helena Senta, Johan E. van Lier, Brigitte Guérin, Roger Lecomte, and Éric E. Turcotte

Sherbrooke Molecular Imaging Center, Research Center of the Sherbrooke University Hospital (CRCHUS), and Department of Nuclear Medicine and Radiobiology, Faculty of Medicine and Health Sciences, Université de Sherbrooke, Sherbrooke, Québec, Canada

After encouraging preclinical and human dosimetry results for the novel estrogen receptor (ER) PET radiotracer 4-fluoro-11β-methoxy-16α-^{18}F-fluoroestradiol (^{18}F-4FMFES), a phase II clinical trial was initiated to compare the PET imaging diagnostic potential of ^{18}F-4FMFES with that of 16α-^{18}F-fluoroestradiol (^{18}F-FES) in ER-positive (ER+) breast cancer patients. **Methods:** Patients diagnosed with ER+ breast cancer (n = 31) were recruited for this study, including 6 who underwent mastectomy or axillary node dissection. For each patient, ^{18}F-FES and ^{18}F-4FMFES PET/CT scans were done sequentially (within a week) and in random order. One hour after injection of either radiotracer, a head-to-thigh static scan with a 2-min acquisition per bed position was obtained. Blood samples were taken at different times after injection to assess each tracer metabolism by reverse-phase thin-layer chromatography. The SUV_{mean} of nonspecific tissues and the SUV_{max} of the tumor were evaluated for each detected lesion, and tumor-to-nonspecific organ ratios were calculated. **Results:** Blood metabolite analysis 60 min after injection of the tracer showed a 2.5-fold increase in metabolic stability of ^{18}F-4FMFES over ^{18}F-FES. Although for most foci ^{18}F-4FMFES PET had an SUV_{max} similar to that of ^{18}F-FES PET, tumor contrast improved substantially in all cases. Lower uptake was consistently observed in nonspecific tissues for ^{18}F-4FMFES, notably a 4-fold decrease in blood-pool activity as compared with ^{18}F-FES. Consequently, image quality was considerably improved using ^{18}F-4FMFES, with lower overall background activity. As a result, ^{18}F-4FMFES successfully identified 9 more lesions than ^{18}F-FES. **Conclusion:** This phase II study with ER+ breast cancer patients showed that ^{18}F-4FMFES PET achieves a lower nonspecific signal and better tumor contrast than ^{18}F-FES PET, resulting in improved diagnostic confidence and lower false-negative diagnoses.

Key Words: receptor PET imaging; ER+; breast cancer; ^{18}F-FES; ^{18}F-4FMFES

J Nucl Med 2018; 59:197–203
DOI: 10.2967/jnumed.117.194654

Knowledge of the estrogen receptor (ER) status is of the utmost importance for the prognosis and choice of treatment modality in breast cancer. Although biopsy is the gold standard to determine ER status in the clinic, substantial effort has been made to assess this parameter noninvasively. 16α-^{18}F-fluoroestradiol (^{18}F-FES) was successfully used in combination with PET imaging to detect ER-positive (ER+) breast cancers in preclinical (*1–3*) and clinical (*4–7*) settings. ^{18}F-FES uptake was shown to correlate well with ER concentrations (*6*) and ER expression as analyzed by the immunohistochemistry index (*8,9*) but not with ER gene expression (*9*). ^{18}F-FES PET imaging was used in a clinical study to follow ER modulation of metastatic breast cancers under different hormone therapies (*10*). Furthermore, functional imaging of ER+ endometrial cancers was demonstrated using ^{18}F-FES PET (*11*), and in combination with ^{18}F-FDG PET, it was possible to assess the aggressiveness of such carcinomas (*12*).

Despite the demonstrated usefulness of ^{18}F-FES for whole-body monitoring of ER status in gynecologic cancers, this tracer still has some shortcomings. First, ^{18}F-FES is rapidly metabolized in the liver by formation of gluconate and sulfate conjugates (*13*), which results in an increase in low-affinity radiometabolites in the blood and nonspecific tissues. As a result, nonspecific background activity is increased, particularly in the mediastinal region, reducing the tumor contrast and the overall image quality. Second, steroid-based tracers such as ^{18}F-FES are bound to have strong hepatic uptake and biliary excretion, resulting in high background activity in the liver and intestines, which could impair detection of lesions in those regions. Third, ^{18}F-FES has affinity to plasma globulins such as sex hormone–binding globulin and albumin, and the percentage of bound ^{18}F-FES depends mainly on the plasma concentration of sex hormone–binding globulin. Since globulin-bound ^{18}F-FES is not available to target the receptors, sex hormone–binding globulin level is inversely correlated with tumoral ^{18}F-FES uptake (*14*), and moreover is likely to contribute to the blood pool.

To improve the metabolic stability and overall performance of ^{18}F-FES for ER imaging, many modifications of the parent estradiol molecule were made and the biologic effect evaluated over the past few decades (*15–18*). A series of 11β-methoxy– or A-ring fluorine–substituted ^{18}F-FES derivatives were synthesized by our research group (*19–21*). Among these derivatives, in vivo assays showed that a combination of 4-fluoro and 11β-methoxy substitution of ^{18}F-FES (e.g., 4-fluoro-11β-methoxy-16α-^{18}F-FES [^{18}F-4FMFES]) displayed the highest uterine uptake and uterus-to-blood ratios in female rats (*22*). This study also reported that ^{18}F-4FMFES shows lower affinity for plasmatic globulins. Further preclinical evaluation on tumor-bearing mice revealed that ^{18}F-4FMFES gave the best in vivo ER+ tumor uptake and image contrast (*23,24*). Subsequently,

Received Apr. 10, 2017; revision accepted Jun. 26, 2017.
For correspondence or reprints contact: Éric E. Turcotte, Nuclear Medicine and Radiobiology, Sherbrooke Molecular Imaging Center, 3001, 12th Ave., Sherbrooke, Québec, Canada, J1H 5N4.
E-mail: eric.e.turcotte@usherbrooke.ca
Published online Aug. 10, 2017.

in a clinical phase I study, substantial uterine uptake and retention were observed in healthy women, with a faster blood clearance and lower uptake in most nonspecific organs, along with hepatobiliary excretion similar to that observed with ^{18}F-FES (*25*).

After these encouraging results, a phase II study was initiated on recently diagnosed ER+ breast cancer patients to directly compare the performance of ^{18}F-4FMFES PET with that of ^{18}F-FES PET. A time-dependent blood metabolite analysis was performed to assess the rate of metabolism of both tracers. Static PET imaging was performed using both tracers for each patient in a 7-d interval. Finally, tumor and nonspecific organ uptake was measured using SUV_{max} and SUV_{mean}, respectively, and tumor-to-nontarget ratios were calculated.

MATERIALS AND METHODS

The study was performed under the authority of Health Canada and approved by the Sherbrooke University Hospital clinical research ethics committee and institutional board, and all subjects signed a written informed consent form. Eligible patients were recruited after either biopsy or resection of the primary and axillary lymph nodes as recommended by the oncologists. Eligibility criteria included patients with newly diagnosed breast cancer at least 1 cm in size, with histologically confirmed ER+ status and suspicion of recurrence. Exclusion criteria included active infection, pregnancy, and concomitant endocrine therapy. In total, 31 patients were examined using both ^{18}F-FES and ^{18}F-4FMFES PET. Six patients were imaged after they underwent mastectomy or axillary dissection to assess whether unsuspected off-site lesions were present. An oncology board staged the patients according to clinical data available before ER PET imaging. Table 1 summarizes the patient characteristics in more detail.

Radiochemistry

^{18}F was prepared by the $^{18}O(p,n)^{18}F$ reaction on ^{18}O-enriched water as target material using the TR-19 or TR-24 cyclotrons (Advanced Cyclotron Systems, Inc.) of the Sherbrooke Molecular Imaging Center. The methods used for the synthesis of ^{18}F-FES have been previously reported (*26*). The precursor for ^{18}F-4FMFES was synthesized as previously described (*20*), whereas labeling at the 16α-position was accomplished via nucleophilic substitution with ^{18}F-F^- on the reactive 16β,17β-cyclic sulfate intermediate (*22*) using an optimized automated procedure (*26*). The preparation, formulation, and quality control procedures of ^{18}F-4FMFES batches were as described previously (*27*). Specific activities of both tracers were similar to or higher than those reported in the literature (*25–27*).

Blood Metabolite Measurement

Blood samples (1 mL each) from the first 10 patients were withdrawn at 1, 2, 3, 5, 10, 20, 30, and 60 min after injection of the imaging dose of either ^{18}F-FES or ^{18}F-4FMFES. Blood was centrifuged at 3,000*g,* and plasma was collected. Five volumes of 99% methanol were added to the plasma samples, which were then centrifuged at 7,500*g* to precipitate proteins. Supernatants and the appropriate diluted standard tracer solution were deposited on a 20 × 20 cm preparative C18 reverse-phase thin-layer chromatography (TLC) plate (Whatman; GE Healthcare) and then eluted for 1 h in a mixture of methanol/water/glacial acetic acid (85:14.6:0.4). Radioactivity on the TLC plates was detected using an Electronic Autoradiography Instant Imager (Canberra Packard) and analyzed by region-of-interest (ROI) drawing of the individual tracer band and the complete migration lane using the Imager software (Canberra Packard). The ratios of the ^{18}F-FES or ^{18}F-4FMFES activities compared with total radioactivity were calculated and expressed as percentage intact radiotracer remaining for each assessed time point.

TABLE 1
Characteristics of ER+ Breast Cancer Patients Included in the Clinical Study

Parameter	Data
Patients (*n*)	31
Age (y)	54.9 ± 10.9 (median, 57; range, 26–73)
Premenopausal (*n*)	8
Detected tumors (*n*)	105
Histology	
Ductal	22 patients, 78 foci
Lobular	5 patients, 9 foci
Other	4 patients, 18 foci
PR-positive	28 patients
HER2-positive	2 patients
Clinical stage	
I	12 patients, 39 foci
II	9 patients, 20 foci
III	5 patients, 18 foci
IV	4 patients, 21 foci
Not determined	1 patient, 1 focus
Node/metastatic status	
N1	12 patients
N2	7 patients
N3-positive	5 patients
M1	10 patients
Surgery status	
Presurgery	25 patients
Postsurgery	6 patients (5 ^{18}F-FES– and ^{18}F-4FMFES–negative)

PR = progesterone receptor; HER2 = human epidermal growth factor receptor 2.

PET Imaging

Patients were injected intravenously with 189.5 ± 17.5 MBq of ^{18}F-FES or 189.4 ± 11.8 MBq of ^{18}F-4FMFES in a total volume of 5–8 mL of physiologic saline (0.9% NaCl), either in the arm contralateral to the primary lesion or in the foot, using a catheter; thereafter, the line was flushed with 20 mL of saline. Each patient was scanned with both tracers, with an interval ranging from 1 to 7 d between scans, selected in a random order. Patients were allowed to stand up, void, and rest in a way compatible with the blood sampling. All acquisitions were performed using a Gemini TF PET/CT scanner (Philips) from midthigh to vertex, including the upper limbs. One hour after injection, a low-dose CT acquisition was initiated, followed immediately by a PET acquisition (7–9 overlapping bed positions, 2 min each). All PET images were reconstructed using a 3-dimensional time-of-flight weighted line-of-response row-action maximum-likelihood algorithm, with attenuation correction derived from the CT attenuation map. The accuracy of the absolute count calibration of the scanner was validated against a uniform phantom containing ^{18}F at a known concentration. The measured activity was expressed as SUV (measured tissue activity concentration/injected activity/patient weight) for each voxel (64 μL).

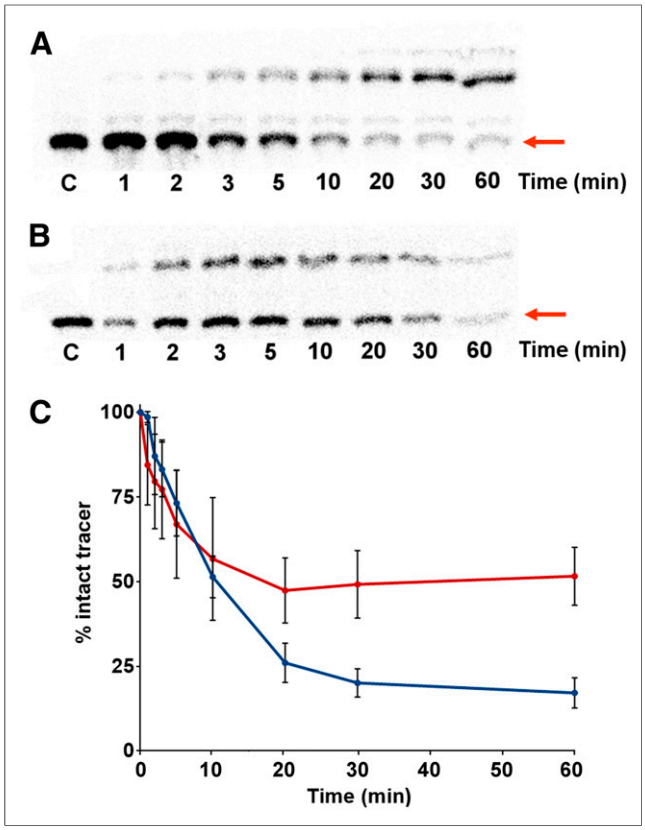

FIGURE 1. Relative metabolite quantification in plasma after injection of either ^{18}F-FES or ^{18}F-4FMFES. (A and B) Representative autoradiography of reverse-phase TLC of multiple blood samplings through time after injection of either ^{18}F-FES (A) or ^{18}F-4FMFES (B). Band corresponding to intact tracer (red arrow) is compared with total radioactivity for each lane. (C) Tracer–to–total radioactivity ratio is expressed as percentage intact tracer. ^{18}F-4FMFES (red curve) has significantly higher percentage intact tracer than ^{18}F-FES (blue curve) at 20 min and afterward ($n = 10$; $P < 0.001$).

Data Analysis

ROIs were drawn and uptake values obtained using MIM software, version 6.0 (MIM Software Inc.). Detectable tumor foci were defined by different ROIs, and a list of organs was assessed, including the cardiac left ventricular cavity (blood), muscle and fat (thigh), and bone (vertebrae), as well as the brain, healthy breast and axillary tissues, lungs, and uterus. The maximum-intensity voxel (SUV_{max}) was taken for tumor and uterine ROI quantification, whereas the averaged value of the voxels included in the ROIs (SUV_{mean}) was used for nontarget organs. Tumor contrast was evaluated by the ratio of tumor uptake to muscle, blood, and fat uptake, as well as to the background value near the lesion. Lesions with a ratio of less than 2.0 were considered equivocal.

Statistical Analysis

Data are reported as mean ± SD. Prism software, version 7.0 (GraphPad Software Inc.), was used to perform statistical analyses and to graph data. Two-way ANOVA using the Sidak method for multiple comparisons was applied to compare ^{18}F-4FMFES and ^{18}F-FES uptake in tumors and nonspecific tissues. The same statistical method was used to compare the tumor-to-nontarget ratios of each tracer. The threshold for significance was a priori set to a P value of less than 0.05.

RESULTS

Blood Metabolites

Reversed-phase TLC autoradiographs of methanol-treated plasma samples from the first 10 patients injected with either ^{18}F-FES or ^{18}F-4FMFES are shown in Figures 1A and 1B, respectively. In both cases, the presence of traces of radiometabolites as early as 1 min after administration is evident. Qualitative observation revealed that although ^{18}F-FES produced up to 3 different more polar metabolites, ^{18}F-4FMFES displayed only 1 radiometabolite of higher polarity.

Changes in the rate of metabolism, as assessed by comparing the activity of the tracer on the TLC plate to the remaining activity in the migration lane, are presented in Figure 1C. During the first 10 min after injection, both radiotracers were degraded at a similar rate. However, whereas the amount of intact ^{18}F-FES continued to drop steadily to about 20%, the ^{18}F-4FMFES metabolite formation plateaued after 10 min after injection. The percentage of intact ^{18}F-4FMFES remained 2- to 2.5-fold higher ($P < 0.001$) than that of ^{18}F-FES during the 20- to 60-min period.

PET Imaging of Patients

Typical examples of PET images obtained with ^{18}F-FES and ^{18}F-4FMFES, for the same patient, are depicted in Figures 2 and 3. The 2 tracers have similar hepatobiliary metabolism and excretion patterns, revealing comparable liver and intestinal radioactivity accumulation. Another common feature, which was noted earlier with other steroid-based radiotracers (*28*), is the tendency of both radiopharmaceuticals to accumulate in variable quantities in the vein proximal to the site of injection. However, overall background activity is visually lower and more uniform using ^{18}F-4FMFES than using ^{18}F-FES. This difference is best exemplified by the images obtained of the heart region (Figs. 3B and 3C). The whole mediastinal and thoracic region reveals a lower and more uniform activity using ^{18}F-4FMFES than using ^{18}F-FES, reflecting the lower concentration of the former in the blood pool and nontarget tissues.

^{18}F-4FMFES PET allowed detection of all ER+ lesions that were also successfully identified with ^{18}F-FES PET. Furthermore, whereas ^{18}F-FES PET identified a total of 96 ER+ lesions, ^{18}F-4FMFES succeeded in detecting an additional 9 lesions, which translates into an 8.6% increase in the detection rate. Those supplemental findings were confirmed as being ER+ breast carcinomas by immunohistochemistry when biopsy was possible, and the presence of a lesion was later assessed by either ^{18}F-FDG PET/CT or bone scintigraphy. Of the 6 postsurgery patients enrolled in the study, 5 were shown to be negative with either ^{18}F-FDG, ^{18}F-FES, or ^{18}F-4FMFES PET. Overall, our data indicate that ^{18}F-4FMFES PET provides better image contrast than ^{18}F-FES PET for the assessment of

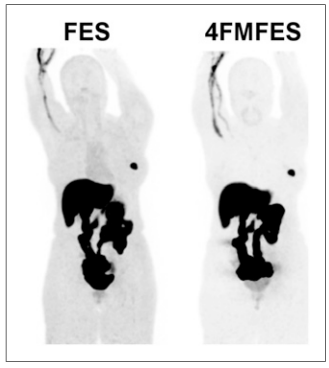

FIGURE 2. Typical maximum-intensity-projection PET images of patient with ER+ primary lesion after injection of either ^{18}F-FES or ^{18}F-4FMFES. Voxel saturation is set to same level for each image. Both tracers show hepatobiliary excretion that generates high background signal to liver and intestines. Less overall background is visible using ^{18}F-4FMFES than using ^{18}F-FES, especially in mediastinal region.

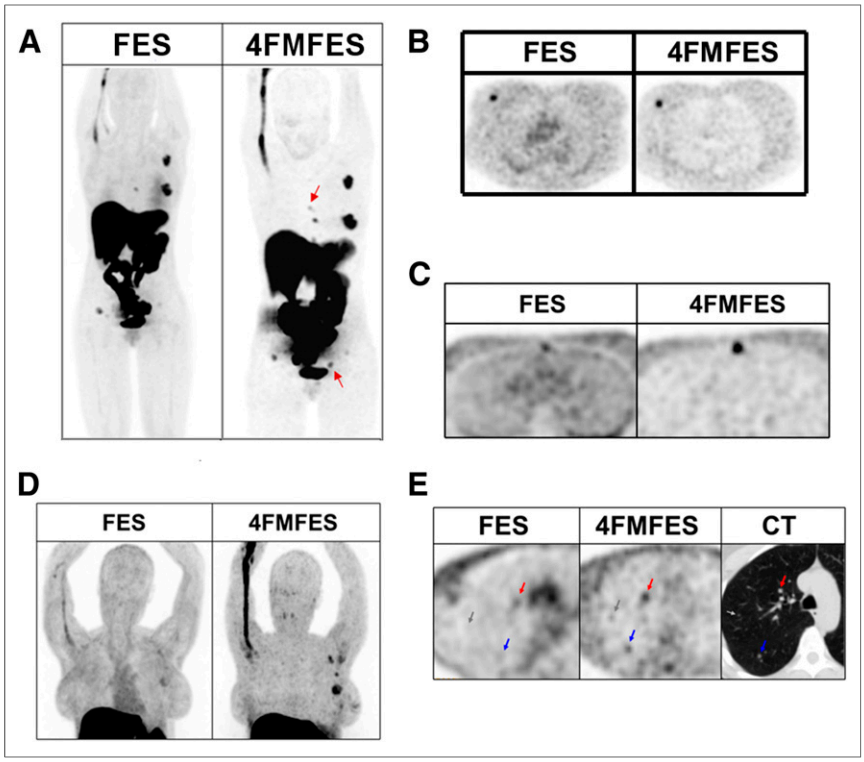

FIGURE 3. Examples of comparative ^{18}F-FES and ^{18}F-4FMFES PET images. Voxel saturation is same for ^{18}F-FES as for ^{18}F-4FMFES in A–C; in D and E, contrast was magnified in ^{18}F-4FMFES PET images for better clarity. (A) Whole-body maximum-intensity-projection PET images of patient initially staged T1cN2M0, in whom ^{18}F-FES PET discovered sternal and iliac bone metastases. ^{18}F-4FMFES PET revealed 2 more foci (arrows) not visible using ^{18}F-FES PET. (B) Typical transaxial slice of primary lesion. Tumor contrast is improved compared with surrounding breast tissue using ^{18}F-4FMFES instead of ^{18}F-FES PET. Mediastinal background activity is reduced using ^{18}F-4FMFES. (C) Transaxial slice of sternal metastasis. Although lesion was considered equivocal with ^{18}F-FES PET, it was readily identified as ER+ foci using ^{18}F-4FMFES PET. (D) Thoracic maximum-intensity projection of patient with suspected recurrence after resection. Although ^{18}F-FES PET reported presence of 2 tumor-infiltrated lymph nodes with equivocal signal, ^{18}F-4FMFES PET revealed 4 distinct ER+ foci. Axillary dissection confirmed presence of lobular carcinoma in suspected sites. (E) ^{18}F-FES and ^{18}F-4FMFES transaxial slices of lung metastatic burden. CT image indicated presence of 5-mm (red arrow), 4-mm (blue arrow), and 2-mm (gray arrow) tumors. ^{18}F-FES PET failed to detect 2 smaller lesions, whereas ^{18}F-4FMFES succeeded in distinguishing all 3 foci (although 2 were equivocal).

ER+ breast cancer, with a higher detection rate of metastases and less thoracic and axillary background radioactivity.

Semiquantitative PET Analysis

Tumor and nontarget organ uptake of ^{18}F-FES and ^{18}F-4FMFES was analyzed and averaged over the corresponding ROIs in all patients. The results are shown in Figure 4 for tumors and in Figure 5 for nontarget tissues. The average SUV_{max} of all assessed lesions did not show any significant difference between ^{18}F-4FMFES and ^{18}F-FES. No other uptake dissimilarities between the 2 tracers were detected when analyzing the primary, axillary, and distant metastasis subgroups, nor did we observe differences in tumor SUVs between pre- and postmenopausal patients. Uterine uptake followed the same trend, with no significant differences being observed between ^{18}F-FES and ^{18}F-4FMFES uptake, regardless of the menopausal status.

In contrast to the similar tumor-targeting properties of both probes, the distribution activity for ^{18}F-4FMFES was substantially and significantly lower than that for ^{18}F-FES in all assessed nontarget organs. In particular, blood-pool activity was 4-fold lower for ^{18}F-4FMFES than for ^{18}F-FES. The reduction in overall background activity was in line with the observed improved overall image contrast with ^{18}F-4FMFES PET, especially in the mediastinal area.

Consequently, tumor-to-blood ($P < 0.0001$), tumor-to-muscle ($P < 0.05$), tumor-to-fat ($P < 0.0001$), and tumor-to-background ($P < 0.05$) ratios were all significantly higher for ^{18}F-4FMFES than for ^{18}F-FES (Fig. 6), with the most noticeable difference (4-fold) being in the tumor-to-blood ratio. Primary, axillary, and metastatic subsets all saw an improvement in their tumor-to-nontarget ratios with ^{18}F-4FMFES PET but reached significance only for tumor-to-blood ratio (all subgroups except lungs) and tumor-to-fat ratio (except lungs and bone subgroups). Moreover, 9 of the lesions detected with ^{18}F-FES were considered equivocal, whereas only 3 of the lesions had a tumor-to-background ratio lower than 2 using ^{18}F-4FMFES. Of those 3 tumors borderline-detectable with ^{18}F-4FMFES, 2 were negative using ^{18}F-FES. This quantitative contrast improvement is responsible for the easier detection of low-ER+ or smaller lesions, as well as for the higher overall rate of detection observed in our small patient sample.

DISCUSSION

ER status is one of the most important prognostic factors in breast cancer management, with ERs having to be present for endocrine therapy to be successful (*29*). Discrepancies between the receptor status of the primary tumor and that of distant metastases were found in up to 40% of patients in retrospective studies (*30,31*). However, it is impractical to take biopsy samples of every known lesion, especially at sites of distant metastasis. Also, considering that ER status can change at recurrence (*32*) or during therapy (*33*), alternative methods for whole-body ER detection are needed. The most successful and sensitive method known so far is ^{18}F-FES PET, which was demonstrated to correlate well with ER status and immunohistochemistry-derived levels of expression (*6,8,9*). Recently, ^{18}F-FES PET was shown to be successful in predicting early progression during fulvestrant therapy (*34*) and contributed to identifying antihormone-resistant breast cancer patients (*35*).

In our study, ^{18}F-4FMFES was evaluated in a clinical phase II trial and compared with the well-known ^{18}F-FES. The 2 tracers exhibited similar tumor uptake, and all lesions detected with ^{18}F-FES were also revealed using ^{18}F-4FMFES. More interestingly, 8.6% more foci were detected by ^{18}F-4FMFES PET than by ^{18}F-FES PET, all of which were later confirmed as true-positive by biopsy sampling or ^{18}F-FDG PET/CT. In addition, 9 axillary, mediastinal, and bone metastases that were difficult to distinguish from the environing background with ^{18}F-FES were more readily detected by ^{18}F-4FMFES

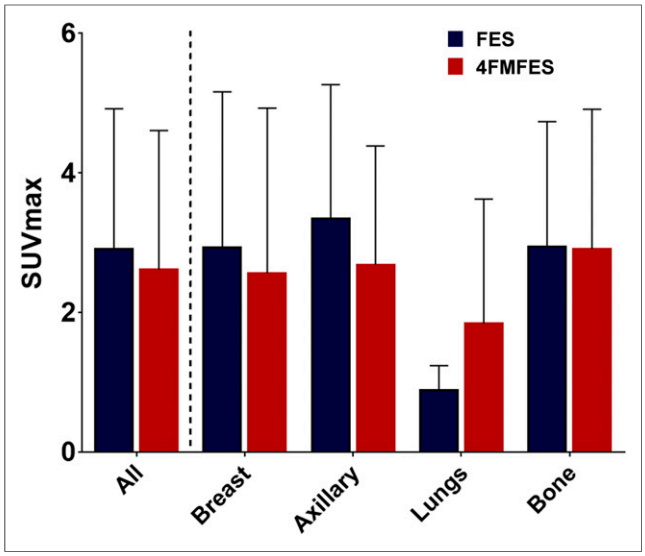

FIGURE 4. ^{18}F-FES and ^{18}F-4FMFES uptake of assessed tumors, expressed as SUV_{max} of representative ROIs. More tumors were identified using ^{18}F-4FMFES PET (n = 105) than ^{18}F-FES PET (n = 96). Although small trend toward lower uptake with ^{18}F-4FMFES PET was observed, difference was not significant, nor did segmentation of tumor pool according to site of presentation show significantly different uptake.

PET. Thus, despite comparable tumor targeting, ^{18}F-4FMFES displayed superior imaging properties due to decreased overall background activity.

This finding was further supported by semiquantitative analyses. Although the 2 tracers exhibited a similar tumor and uterine SUV_{max}, uptake in all assessed nontarget organs and tissues was significantly lower with ^{18}F-4FMFES than with ^{18}F-FES, in accordance with the overall qualitative aspect of the produced images, and explaining the increased detection rate with ^{18}F-4FMFES.

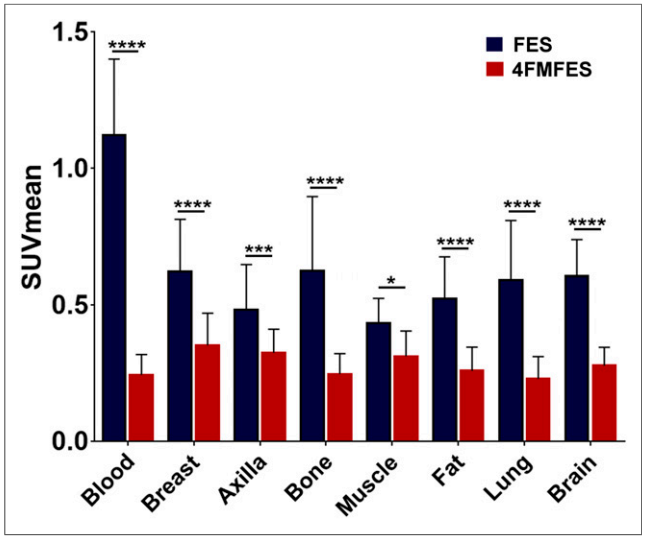

FIGURE 5. ^{18}F-FES and ^{18}F-4FMFES uptake of nontarget reference tissues, expressed as SUV_{mean} of representative ROIs. Blood pool was assessed by ROI drawn into left ventricular cavity. Breast and axilla ROIs were drawn contralateral to primary lesion. Muscle and fat ROIs were derived from thigh. ^{18}F-4FMFES consistently presented significantly lower uptake than ^{18}F-FES in all assessed reference tissues (n = 31). *$P < 0.05$. ***$P < 0.005$. ****$P < 0.001$.

Many factors explain the improved imaging properties of ^{18}F-4FMFES. This novel ER PET tracer was initially designed to improve in vivo stability by the introduction of a second (nonradioactive) fluorine at position 4 of the steroid A-ring (*36*). Furthermore, to decrease nonspecific binding to plasma globulins, an 11β-methoxy moiety was added to the parent ^{18}F-FES (*16,22*). The improved properties are indeed reflected in the observed distribution pattern of ^{18}F-4FMFES versus ^{18}F-FES. First, plasma metabolite analysis at, for example, 1 h after injection—the optimal time for static PET imaging—revealed a 2.5-fold increase in intact ^{18}F-4FMFES as compared with ^{18}F-FES. Moreover, whereas 3 new radiometabolites were observed by radio-TLC with samples of ^{18}F-FES, only one ^{18}F-4FMFES–derived radiometabolite was revealed. The nature of the different metabolites was not further studied, but previous work from Mankoff et al. (*13*) on ^{18}F-FES identified mainly sulfate and glucuronide addition, which is in line with our finding that all metabolites we observed were more polar than the parent tracer. Although ^{18}F-4FMFES, because of the presence of fluoro substituents proximal to the expected metabolic sites, was deemed impervious to such processing, it may be possible that one of the steroidal hydroxyl groups is still modifiable by hepatic enzymes.

Second, binding to plasma globulins slows the metabolic and blood clearance rates of steroids (*28,37*). Hence, the lack of ^{18}F-4FMFES binding affinity for sex hormone–binding globulin may facilitate its release from the blood pool, resulting in lower background activity than for ^{18}F-FES. Moreover, ^{18}F-4FMFES is more lipophilic than ^{18}F-FES, potentially further accelerating blood clearance (*38*). Thus, notwithstanding the lower in vitro ER binding affinity of ^{18}F-4FMFES (*22*) and similar tumor uptake of ^{18}F-4FMFES and ^{18}F-FES in patients, the 2.5-fold increase in stability of ^{18}F-4FMFES (despite the lack of sex hormone–binding globulin binding), compared with ^{18}F-FES, likely explains the substantial gain in tumor contrast obtained with ^{18}F-4FMFES versus ^{18}F-FES.

Another factor to consider is that blood estradiol levels were not monitored before imaging, nor did we consider the effect of the menstrual cycle for the premenopausal women. However, tumor, uterine, and nontarget organ SUVs did not significantly differ between pre- and postmenopausal patients, suggesting that circulating estradiol did not substantially affect tumor targeting. This possibility agrees with earlier observations defining confounding factors in ^{18}F-FES PET imaging, where patients with an estradiol level of more than 30 pg/mL did not have significantly lower ^{18}F-FES tumor SUVs than patients with low estrogen levels (*39*).

CONCLUSION

In this preliminary clinical phase II study, we showed that the novel ER PET tracer ^{18}F-4FMFES achieved tumor uptake similar to, but nonspecific organ and blood retention lower than, that of ^{18}F-FES. Hence, ^{18}F-4FMFES PET allowed higher detection rates and better sensitivity than its parent, ^{18}F-FES, toward ER+ breast carcinomas. Further investigations are in progress to evaluate the potential of ^{18}F-4FMFES PET to assess recurrence, treatment follow-up, sensitivity, specificity, and accuracy and to complement classic ^{18}F-FDG PET in breast cancer diagnosis and follow-up.

DISCLOSURE

This work was supported by the Canadian Breast Cancer Foundation (CBCF). Johan E. van Lier, Brigitte Guérin, Roger

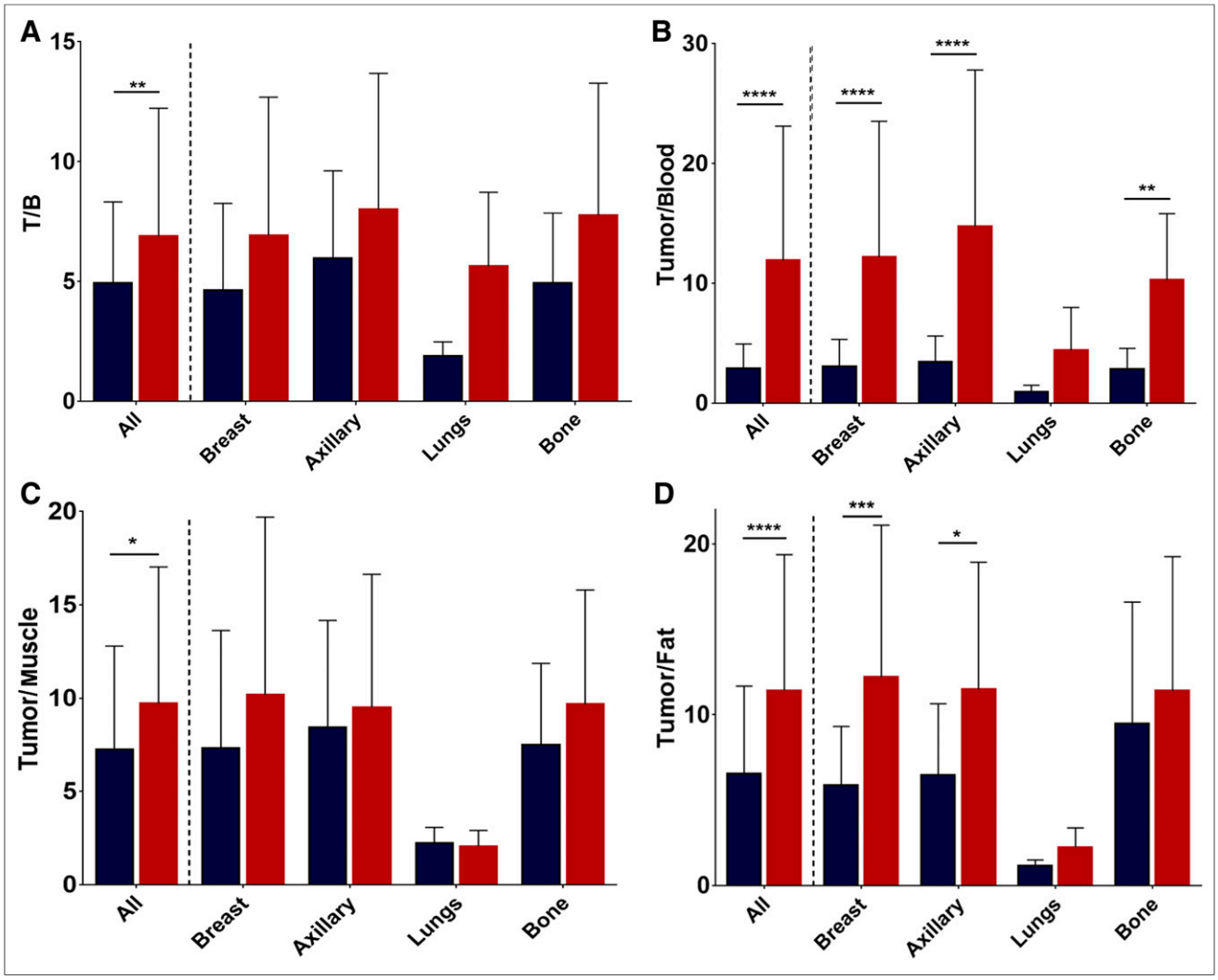

FIGURE 6. ^{18}F-FES (blue) and ^{18}F-4FMFES (red) tumor-to-background (T/B) (A), tumor-to-blood (B), tumor-to-muscle (C), and tumor-to-fat (D) ratios. ^{18}F-4FMFES achieved significantly better tumor contrast than ^{18}F-FES regardless of nonspecific tissue of reference. Significantly higher tumor-to-blood and tumor-to-fat ratios were also observed for ^{18}F-4FMFES when subcategorizing tumor pool according to tumor site. $^{*}P < 0.05$. $^{**}P < 0.01$. $^{***}P < 0.005$. $^{****}P < 0.001$.

Lecomte, and Éric E. Turcotte are members of the Research Center of the CHUS (CRCHUS), Sherbrooke, Quebec, Canada, supported by the Fonds de la Recherche du Québec–Santé (FRQ-S). No other potential conflict of interest relevant to this article was reported.

REFERENCES

1. Aliaga A, Rousseau JA, Ouellet R, et al. Breast cancer models to study the expression of estrogen receptors with small animal PET imaging. *Nucl Med Biol.* 2004;31:761–770.
2. Paquette M, Ouellet R, Archambault M, Croteau E, Lecomte R, Benard F. [^{18}F]-fluoroestradiol quantitative PET imaging to differentiate ER+ and ERα-knockdown breast tumors in mice. *Nucl Med Biol.* 2012;39:57–64.
3. He S, Wang M, Yang Z, et al. Comparison of ^{18}F-FES, ^{18}F-FDG, and ^{18}F-FMISO PET imaging probes for early prediction and monitoring of response to endocrine therapy in a mouse xenograft model of ER-positive breast cancer. *PLoS One.* 2016;11:e0159916.
4. Mintun MA, Welch MJ, Siegel BA, et al. Breast cancer: PET imaging of estrogen receptors. *Radiology.* 1988;169:45–48.
5. Dehdashti F, Mortimer JE, Siegel BA, et al. Positron tomographic assessment of estrogen receptors in breast cancer: comparison with FDG-PET and in vitro receptor assays. *J Nucl Med.* 1995;36:1766–1774.
6. Mortimer JE, Dehdashti F, Siegel BA, Katzenellenbogen JA, Fracasso P, Welch MJ. Positron emission tomography with 2-[^{18}F]fluoro-2-deoxy-D-glucose and 16α-[^{18}F]fluoro-17β-estradiol in breast cancer: correlation with estrogen receptor status and response to systemic therapy. *Clin Cancer Res.* 1996;2:933–939.
7. Kumar P, Mercer J, Doerkson C, Tonkin K, McEwan AJ. Clinical production, stability studies and PET imaging with 16-alpha-[^{18}F]fluoroestradiol ([^{18}F]FES) in ER positive breast cancer patients. *J Pharm Pharm Sci.* 2007;10(suppl):256s–265s.
8. Peterson LM, Mankoff DA, Lawton T, et al. Quantitative imaging of estrogen receptor expression in breast cancer with PET and ^{18}F-fluoroestradiol. *J Nucl Med.* 2008;49:367–374.
9. Gemignani ML, Patil S, Seshan VE, et al. Feasibility and predictability of perioperative PET and estrogen receptor ligand in patients with invasive breast cancer. *J Nucl Med.* 2013;54:1697–1702.
10. Linden HM, Kurland BF, Peterson LM, et al. Fluoroestradiol positron emission tomography reveals differences in pharmacodynamics of aromatase inhibitors, tamoxifen, and fulvestrant in patients with metastatic breast cancer. *Clin Cancer Res.* 2011;17:4799–4805.
11. Tsujikawa T, Yoshida Y, Kiyono Y, et al. Functional oestrogen receptor α imaging in endometrial carcinoma using 16α-[^{18}F]fluoro-17β-oestradiol PET. *Eur J Nucl Med Mol Imaging.* 2011;38:37–45.
12. Tsujikawa T, Yoshida Y, Kudo T, et al. Functional images reflect aggressiveness of endometrial carcinoma: estrogen receptor expression combined with ^{18}F-FDG PET. *J Nucl Med.* 2009;50:1598–1604.

13. Mankoff DA, Tewson TJ, Eary JF. Analysis of blood clearance and labeled metabolites for the estrogen receptor tracer [F-18]-fluorestradiol (FES). *Nucl Med Biol.* 1997;24:341–348.
14. Tewson TJ, Mankoff DA, Peterson LM, et al. Interactions of 16alpha-[^{18}F]-fluoroestradiol (FES) with sex steroid binding protein (SBP). *Nucl Med Biol.* 1999;26:905–913.
15. Kiesewetter DO, Kilbourn MR, Landvatter SW, Heiman DF, Katzenellenbogen JA, Welch M. Preparation of four fluorine-18-labeled estrogens and their selective uptakes in target tissues of immature rats. *J Nucl Med.* 1984;25:1212–1221.
16. Pomper MG, VanBrocklin H, Thieme AM, et al. 11-beta-methoxy-, 11-beta-ethyl- and 17-alpha-ethynyl-substituted 16-alpha-fluoroestradiols: receptor-based imaging agents with enhanced uptake efficiency and selectivity. *J Med Chem.* 1990;33:3143–3155.
17. Ali H, Rousseau J, van Lier JE. Synthesis of A-ring fluorinated derivatives of (17α,20E/Z)-[^{125}I]iodovinylestradiols: effect on receptor binding and receptor-mediated target tissue uptake. *J Med Chem.* 1993;36:3061–3072.
18. Katzenellenbogen JA. The 2010 Philip S. Portoghese Medicinal Chemistry Lectureship: addressing the "core issue" in the design of estrogen receptor ligands. *J Med Chem.* 2011;54:5271–5282.
19. Ali H, Rousseau J, Gantchev TG, van Lier JE. 2- and 4-fluorinated, 16α-[^{125}I] iodoestradiol derivatives: synthesis and effect on estrogen, receptor binding and receptor-mediated target tissue uptake. *J Med Chem.* 1993;36:4255–4263.
20. Seimbille Y, Ali H, van Lier JE. Synthesis of 2,16α- and 4,16α-difluoroestradiols and their 11β-methoxy derivatives as potential estrogen receptor-binding radiopharmaceuticals. *J Chem Soc Perkin Trans.* 2002;5:657–663.
21. Ahmed N, Garcia G, Ali H, van Lier JE. ^{18}F-labeling of A-ring substituted 16α-fluoro-estradiols as potential radiopharmaceuticals for PET imaging. *Steroids.* 2009;74:42–50.
22. Seimbille Y, Rousseau J, Bénard F, et al. ^{18}F-labeled difluoroestradiols: preparation and preclinical evaluation as estrogen receptor-binding radiopharmaceuticals. *Steroids.* 2002;67:765–775.
23. Bénard F, Ahmed N, Beauregard JM, et al. [^{18}F]Fluorinated estradiol derivatives for oestrogen receptor imaging: impact of substituents, formulation and specific activity on the biodistribution in breast tumour-bearing mice. *Eur J Nucl Med Mol Imaging.* 2008;35:1473–1479.
24. Paquette M, Phoenix S, Ouellet R, et al. Quantitative assessment of the novel estrogen receptor PET tracer 4-fluoro-11β-methoxy-16α-[^{18}F]fluoroestradiol (4FMFES) by PET imaging in a breast cancer murine model. *Mol Imaging Biol.* 2013;15:625–632.
25. Beauregard JM, Croteau E, Ahmed N, van Lier JE, Benard F. Assessment of human biodistribution and dosimetry of 4-fluoro-11β-methoxy-16α-^{18}F-fluoroestradiol using serial whole-body PET/CT. *J Nucl Med.* 2009;50:100–107.
26. Lim JL, Zheng L, Berridge MS, Tewson TJ. The use of 3-methoxymethyl-16-beta, 17-beta-epiestriol-O-cyclic sulfone as the precursor in the synthesis of [^{18}-F]-16α-fluoroestradiol. *Nucl Med Biol.* 1996;23:911–915.
27. Ahmed N, Langlois R, Rodrigue S, Benard F, van Lier JE. Automated synthesis of 11β-methoxy-4,16α-[16α-^{18}F]difluoroestradiol (4F-M[^{18}F]FES) for estrogen receptor imaging by positron emission tomography. *Nucl Med Biol.* 2007;34:459–464.
28. Jonson SD, Bonasera TA, Dehdashti F, Cristel ME, Katzenellenbogen JA, Welch MJ. Comparative breast tumor imaging and comparative in vitro metabolism of 16α-[^{18}F]fluoroestradiol-17β and 16β-[^{18}F]fluoromoxestrol in isolated hepatocytes. *Nucl Med Biol.* 1999;26:123–130.
29. Davies C, Godwin J, Gray R, et al. Relevance of breast cancer hormone receptors and other factors to the efficacy of adjuvant tamoxifen: patient-level meta-analysis of randomised trials. *Lancet.* 2011;378:771–784.
30. Foukakis T, Astrom G, Lindstrom L, Hatschek T, Bergh J. When to order a biopsy to characterise a metastatic relapse in breast cancer. *Ann Oncol.* 2012;23(suppl 10):x349–x353.
31. Lindström LS, Karlsson E, Wilking UM, et al. Clinically used breast, cancer markers such as estrogen receptor, progesterone receptor, and human epidermal growth factor receptor 2 are unstable, throughout tumor progression. *J Clin Oncol.* 2012;30:2601–2608.
32. Kuukasjärvi T, Kononen J, Helin H, et al. Loss of estrogen receptor in recurrent breast cancer is associated with poor response to endocrine therapy. *J Clin Oncol.* 1996;14:2584–2589.
33. Gutierrez MC, Detre S, Johnston S, et al. Molecular changes in tamoxifen-resistant breast cancer: relationship between estrogen receptor, HER-2, and p38 mitogen-activated protein kinase. *J Clin Oncol.* 2005;23:2469–2476.
34. van Kruchten M, de Vries EG, Glaudemans AW, et al. Measuring residual estrogen receptor availability during fulvestrant therapy in patients with metastatic breast cancer. *Cancer Discov.* 2015;5:72–81.
35. van Kruchten M, Glaudemans AW, de Vries EF, Schröder CP, de Vries EG, Hospers GA. Positron emission tomography of tumour [^{18}F]fluoroestradiol uptake in patients with acquired hormone-resistant metastatic breast cancer prior to oestradiol therapy. *Eur J Nucl Med Mol Imaging.* 2015;42:1674–1681.
36. Morgan P, Maggs JL, Bulman-Page PC, Hussain F, Park BK. The metabolism of 2- and 4-fluoro-17-oestradiol in the rat and its implications for oestrogen carcinogenesis. *Biochem Pharmacol.* 1992;43:985–993.
37. Plymate SR, Namkung PC, Matej LA, Petra PH. Direct effect of plasma sex hormone binding globulin (SHBG) on the metabolic clearance rate of 17β-estradiol in the primate. *J Steroid Biochem.* 1990;36:311–317.
38. Lukka PB, Paxton JW, Atwell GJ, Kestell P, Baguley BC. A rapid LC-MS/MS method for the quantitation of a series of benzonaphthyridine derivatives: application to in vivo pharmacokinetic and lipophilicity studies in drug development. *J Pharm Biomed Anal.* 2012;63:9–16.
39. Peterson LM, Kurland BF, Linka JM, et al. Factors influencing the uptake of ^{18}F-fluoroestradiol in patients with estrogen receptor positive breast cancer. *Nucl Med Biol.* 2011;38:969–978.